Available online at www.sciencedirect.com
SCIENCE DIRECT
Polymer 46 (2005) 8819–8837
polymer
www.elsevier.com/locate/polymer

Does the length of the short chain branch affect the mechanical properties of linear low density polyethylenes? An investigation based on films of copolymers of ethylene/1-butene, ethylene/1-hexene and ethylene/1-octene synthesized by a single site metallocene catalyst

Pankaj Gupta[a,1], Garth L. Wilkes[a,*], Ashish M. Sukhadia[b], Rajendra K. Krishnaswamy[b], Mark J. Lamborn[b], Stephen M. Wharry[b], Chung C. Tso[b], Paul J. DesLauriers[b], Todd Mansfield[c], Frederick L. Beyer[d]

[a]*Department of Chemical Engineering, Virginia Polytechnic Institute and State University, Blacksburg, VA 24061, USA*
[b]*Chevron Phillips Chemical Company, Bartlesville, OK, USA*
[c]*Procter and Gamble Company, Cincinnati, OH, USA*
[d]*US Army Research Laboratory, Aberdeen, MD, USA*

Available online 12 July 2005

Abstract

Three nearly identical linear low density polyethylene resins based on copolymers of ethylene with 1-butene (B), 1-hexene (H) and 1-octene (O) were utilized to investigate the effect of short chain branch length on the mechanical properties of blown and compression molded (quenched and slow cooled) films. The content of short chain comononer in the three copolymers was ca. 2.5–2.9 mol% that corresponded to a density of 0.917–0.918 g/cm^3. Within a given series, the tensile properties of these films do not show any significant difference at slow deformation rates (up to 510 mm/min), even though the DSC and TREF profiles of 'H' and 'O' differed slightly in comparison to 'B'. However, at higher deformation rates (ca. 1 m/s), the breaking strength of these films was found to increase with increasing short chain branch length. In addition, the Spencer impact and Elmendorf tear strength of the blown films were also observed to increase with increasing short chain branch length. Further, dart impact strength and high-speed puncture resistance (5.1 m/s) of 1-octene and 1-hexene based samples was also observed to be higher than that based on 1-butene. The blown films displayed low and comparable levels of equivalent in-plane birefringence and crystalline orientation by wide angle X-ray scattering. This confirms that the differences in mechanical properties in the blown film series are not attributable to differences in molecular orientation. The deformation behavior of both the compression molded and blown films were also investigated in a well-defined controlled regime by analyzing their essential work of fracture. It was found that the essential work of fracture of films based on 1-hexene and 1-octene was higher than that of films based on 1-butene. While the origin of these differences in mechanical properties with increasing short chain branch length is not fully understood, the present investigation confirms this effect to be pronounced at high deformation rates for both the blown and compression molded quenched films.

Keywords: Polyethylene; Short chain branching; Mechanical

1. Introduction

Linear low density polyethylenes (LLDPEs) are made by the copolymerization of ethylene and an α-olefin, such as 1-butene, 1-hexene, 1-octene, 4-methyl-1-pentene, etc. The α-olefin, present in small amounts in the copolymer, introduces short chain branches (SCB) on the polymer backbone; for instance, the three particularly common comonomers, 1-butene, 1-hexene and 1-octene addressed in this report introduce ethyl, butyl and hexyl branches, respectively. The primary objective of this study is to investigate whether the length of the short chain branch (2.5–2.9 mol%, at a copolymer density of ca. 0.917–0.918 g/cm^3) affects the mechanical properties of LLDPE

* Corresponding author. Tel.: +1 540 231 5498; fax: +1 540 231 9511.
E-mail address: gwilkes@vt.edu (G.L. Wilkes).
[1] Current address: Materials R&D, The Dow Chemical Company, Freeport, 77541, TX, USA.

0032-3861/$ - see front matter © 2005 Elsevier Ltd. All rights reserved.
doi:10.1016/j.polymer.2005.05.137

films. As will be reviewed below, many studies have attempted to address this same topic but in doing so, many important and influential parameters were not necessarily well controlled in the respective investigations. We believe the present report has improved on this aspect as will be discussed.

LLDPE resins are typically produced using Ziegler Natta heterogeneous catalysts, whose origins can be traced back to the late 1950s [1]. However, the resins produced by these catalysts are characterized by considerable heterogeneity in their microstructure and melting behavior and are considered to be a mixture of fractions of polyethylene copolymers with a range of molecular weights and short chain branch content. In the mid 1990s, with the commercial advent of high efficiency single site metallocene catalysts, narrow molecular weight distribution LLDPEs with considerably more homogenous distribution of short chain branches were produced. Metallocene-based LLDPE resins have now been commercialized using various different catalyst technologies [2–6]. The single site metallocene catalysts produce copolymers that have much narrower molecular weight distributions (ca. 2–3) and a greater uniformity in the distribution of the short chain branching across the width of the molecular weight distribution relative to the Ziegler Natta catalyzed systems.

LLDPE resins of all types constitute a major segment of the polyethylene (PE) blown film market worldwide. It is known that the mechanical properties of the LLDPE films are influenced by molecular structural parameters such as molecular weight, molecular weight distribution in addition to the amount as well as the short chain branch distribution (SCBD) across the width of the copolymer molecular weight distribution. Morphological features such as degree of crystallinity, intercrystalline connectivity and preferred orientation are also strongly believed to have an effect of the mechanical properties of blown LLDPE films [7–19].

Short chain branching critically affects the crystallinity and thus the morphology and consequently the solid-state properties of the corresponding LLDPE films. As a result, a broad range of properties of LLDPEs can be obtained by varying the amount of SCB and the SCBD. In addition, the length of the short chain branch may also play an important role in governing the mechanical properties—the specific issue that will be addressed in this study. Early on, Cady [20] investigated the effects of the type of short chain branching (SCB) and SCBD on the dart impact and Elmendorf tear strength of blown films of LLDPEs based on 1-butene, 1-hexene and 1-octene that were synthesized using Zeigler Natta catalyst chemistry. For similar density and melt flow index, the 1-butene based resins performed poorly in comparison to those based on 1-hexene and 1-octene, even though it had a more homogenous SCBD. However, comparison of two different 1-octene based resins that differed in their SCBD indicated better mechanical performance for the 1-octene based resin that had a more homogenous SCBD. No comment was made on the relative amounts of the short chain branching in each of the resins, % crystallinity or orientation of the blown films. However, it was concluded that the combination of the short chain branch length and a more homogenous SCBD leads to better mechanical properties of LLDPE blown films. In a similar study utilizing LLDPE resins based on 1-butene, 1-hexene and 1-octene that had densities in the range of 0.919–0.921 g/cm^3, melt flow indices of 0.9–1 dg/min and polydispersities of 3.3–4.1, Liu and Baker [21] observed the impact strength to increase with increasing short chain branch length. It was suggested that the longer short chain branches lead to a larger fraction of tie molecules in the interlamellar region that causes the observed increase in impact strength. However, in this study as well, both the comonomer content and the SCBD varied simultaneously, thereby making the interpretation of the corresponding effects uncertain. In a third study, Kim and Park [22] observed a similar trend for Zeigler-Natta catalyzed 1-butene, 1-hexene and 1-octene based LLDPE blown films that had relatively larger polydispersities ($\sim$6), varying comonomer composition (4.3, 3.7 and 2.8 mol% of 1-butene, 1-hexene and 1-octene, respectively) and varying branch density (21, 17 and 13 CH_3/1000 C for 1-butene, 1-hexene and 1-octene based resins, respectively). The differences in the dart impact and Elmendorf tear strengths of the blown films based on the three resins were attributed to the differences in short chain branching distributions and increased imperfections in the crystallographic order and decreased lamellar thickness with increasing short chain branch length.

Wolfe [23] studied the effect of comonomer type on the slow crack growth resistance of high-density polyethylene using the PENT (ASTM F1473) test. Of the two comonomers investigated ('B' and 'H'), the HDPE based on 1-hexene failed after 400 h compared to 30 h in the case of HDPE based on 1-butene. No comment, however, was made on the molecular weight, distribution of the short chain branches and orientation of molecular chains in the pipe resins utilized.

By investigating LLDPE resins based on 1-butene and 1-octene, Kale et al. [24] compared the intrinsic tear strengths for two sets of resins (each set had two resins based each on 1-butene and 1-octene) of densities 0.912 and 0.921 g/cm^3, respectively. The resins had similar polydispersities (2.12–2.25), melt flow indices (0.93–1.02) but different short chain branch comonomer content. For the 0.912 g/cm^3 set of resins, the mol% of 1-butene was 4.17 and that of 1-octene was 3.04; for the 0.921 g/cm^3 set of resins, these were 3.04 and 1.77 mol%, respectively, for 1-butene and 1-octene. Despite the differences in their comonomer content and the lack of information on the SCBD, the higher intrinsic tear strength of the 1-octene based LLDPE resins relative to the 1-butene based resins was speculated to be due to enhanced tie molecule formation with increasing short chain branch length. Further, the observed difference in the melting point versus mole fraction comonomer relationships for 1-butene and 1-octene based LLDPE resins was suggested to be due to the

incorporation of small amounts of 1-butene into the crystalline phase and/or variations in the commoner sequence distributions. However, Alizadeh et al. [25] and Alamo et al. [26] have shown that the melting point depression with increasing mole fraction of the short chain branch comonomer is independent of the type of the comonomer, i.e. at any given mole fraction of 1-butene, 1-pentene, 1-hexene and 1-octene in metallocene catalyzed copolymers with polyethylene, the melting point depression of all these copolymers was observed to be comparable. Further, Alizadeh et al. [25] observed that at any given mol% of the short chain branch comonomer, the degree of crystallinity was also very comparable for LLDPE based on 1-butene, 1-pentene, 1-hexene and 1-octene. These observations clearly suggest that the degree/probability of branch exclusion from the lamellar crystal is independent of the comonomer type, viz. 1-butene, 1-hexene and 1-octene. Therefore, in turn, one would expect no differences in tie molecule formation for the three LLDPE materials based on 1-butene, 1-hexene and 1-octene.

Kennedy et al. [27] also studied the tensile stress–strain behavior of metallocene catalyzed LLDPE resins based on 1-butene, 1-hexene, 1-octene and 4-methyl-1-pentene. It was observed that the nominal-stress strain curves, that were measured at low deformation rate of 0.0004 m/s (1 in./min) compared to high deformation rates involved during the impact (0.2–4 m/s) and Elmendorf tear testing (0.1–7 m/s), were dominated by strain hardening for all the LLDPEs resins excepting those based on 1-butene. The yield stress and initial modulus were related to the degree of crystallinity regardless of the short chain branch comonomer. More importantly, for the highest molecular weights studied ($M_w > 100{,}000$ g/mol) the force-elongation curves (recorded at low deformation rates of 0.0004 m/s) for the four resins were observed to be similar to one another for the same short chain branch content. This last observation is important for until the present report, the tensile stress strain behavior of LLDPE resins, particularly based on 1-butene, 1-hexene or 1-octene, have not been systematically studied at high deformation rates similar to those involved in dart or Spencer impact and Elmendorf tear strength testing. In addition, the dart or Spencer impact strength and Elmendorf tear resistance measurements, although standard ASTM measurements in industry are characterized by non-uniform deformation rates.

It is important to note that most of the studies that relate to the influence exerted by the branch length involve comparisons of LLDPE films from resins that either have different short chain branch contents, different comonomer distribution profile (SCBD), different polydispersities or different short chain branch density on the main ethylene backbone. As a result, it is extremely difficult to properly interpret the results and separate the effects of the individual parameters (mentioned above) on the physical properties of LLDPE resins due to their simultaneous variation. Thus, in this study, three LLDPE resins based on 1-butene, 1-hexene and 1-octene, that have been carefully synthesized [28] using the same single site metallocene based catalyst, were examined to specifically investigate the effect of the comonomer type (short chain branch length), viz. 1-butene, 1-hexene and 1-octene on the mechanical properties of blown and compression molded LLDPE films. As will be discussed later, these three resins were very comparable in terms of their molecular, rheological, comonomer content and SCBD aspects. As a result, any differences arising out of structural differences from other origins, while not fully eliminated, were minimized. Results from the earlier study [28] showed that while the tensile properties, at nominal deformation rates, of the blown films were indistinguishable, the Elmendorf tear, dart impact and Spencer impact properties of the 1-butene based films were significantly lower than the corresponding 1-hexene and 1-octene based films. The difference between 1-hexene and 1-octene films was much smaller with a slight advantage for the 1-octene films. In this study, we attempt to further investigate the effect of the type of the short chain branch on the mechanical properties of LLDPE films since other parameters (like comonomer content, SCBD, molecular weight, molecular weight distribution, polydispersity and density) were established to be essentially constant [28]. The mechanical properties were measured utilizing Spencer impact, Elmendorf tear resistance and high-speed puncture resistance measurements as well as in a controlled tensile deformation regime by utilizing the essential work of fracture methodology/technique.

2. Essential work of fracture (EWF)

Recent studies have indicated that the EWF procedure is a very useful method to study the fracture properties of thin films and ductile materials [29–33]. The concept of EWF was developed initially by Cotterell and Reddel [34] on the basis of ideas proposed by Broberg [35], who suggested that the total work of fracture (W_f) dissipated in a precracked specimen could be represented as a sum of the work consumed into two distinct zones. As shown in Fig. 1, the double-edge-notched-tension (DENT) specimen that is precracked along the horizontal (inwards from the vertical edges) to leave a ligament region 'l' that undergoes the actual deformation in tension under a load 'F' along the vertical. The regions marked as '1' and '2' depict the fracture process zone (FPZ) and the outer plastic zone, respectively, (OPZ).

The work dissipated in the FPZ corresponds to the essential work of fracture (W_e); and the work required to yield the material in the OPZ is the non-essential work of fracture (W_p) that depends on the geometry of the specimen tested. Thus, the total fracture energy is expressed as (more details are provided elsewhere [34]):

$$W_f = W_e + W_p = w_e l t + w_p \beta l^2 t \quad (1)$$

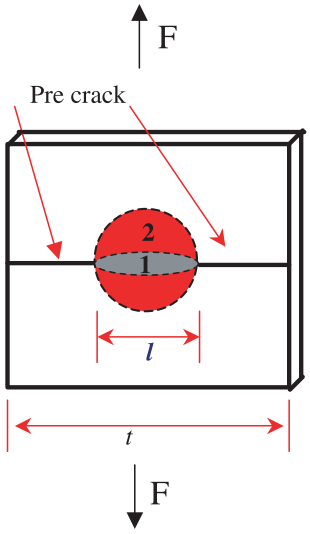

Fig. 1. Sample geometry utilized in the double edge notched tension (DENT) mode. The zones marked with 1 and 2 indicate the fracture process zone (FPZ) and outer plastic zone (OPZ), respectively. The ligament length (denoted as '*l*') in the present study was 1, 2 or 3 mm.

where w_e is the specific essential work of fracture (per unit ligament area), w_p is the specific non-essential work of fracture (per unit volume), l is the ligament length, t is the specimen thickness and β is the plastic zone shape factor. The total specific work of fracture is represented by:

$$w_f = \frac{W_f}{lt} = w_e + \beta w_p l \tag{2}$$

From Eq. (2), it is clear that w_f has a linear relationship with the ligament length. In other words, a plot of the w_f as a function of l should be linear with the intercept on the ordinate axis and the slope providing w_e and βw_p, respectively. Thus, this method involves testing of specimens that have different ligament lengths, and then evaluating the W_f for each specimen (area under the force–displacement curve) followed by suitable normalization with respect to the ligament area to give a plot of w_f vs. l. The best-fit regression line would then give the slope (βw_p) and intercept (w_e).

When plane stress conditions prevail for all ligament lengths, it is assumed [36] that w_e is a material property (a constant) at a given thickness. Mathematically, for plane stress conditions, the following two relationships should be satisfied:

$$l \geq (3 \sim 5)t \tag{3}$$

$$t \ll 25\frac{w_e}{\sigma_y} \tag{4}$$

Under these conditions, it has been demonstrated theoretically [37] and supported experimentally [37–39] that w_e is equivalent to J_c, or the J-integral. For a nonlinear elastic body containing a precrack and undergoing deformation, J_c represents the strain energy release rate of nonlinear elastic materials and is given by: [40]

$$J_C = -\frac{dU}{dA} \tag{5}$$

where U is the potential energy (also the difference between the strain energy stored in the body and the work done by external forces of deformation) and A is the crack area. It can be seen that the units of J_c are also energy/area (the same as w_e). Thus, the advantage of the EWF method is its experimental simplicity as compared to the J-integral procedure.

3. Experimental

3.1. Material synthesis

The three LLDPE copolymers (based on ethylene-*co*-1-butene, 'B', ethylene-*co*-1-hexene, 'H', and ethylene-*co*-1-octene, 'O') used in this study were synthesized by using a Chevron Phillips' proprietary zirconium based metallocene catalyst [28]. The copolymerization was conducted in a pilot plant at Chevron Phillips under steady state slurry-loop copolymerization conditions. The comonomers and the catalyst were fed continuously and the polymer fluff was continuously removed from the reactor. The fluff was purged with nitrogen to remove residual solvent and unreacted olefins followed by blending with antioxidants and a processing aid. The polymers were then extruded into pellets.

3.2. Characterization of the resins

The molecular, rheological and branching characteristics of the three resins are listed in Table 1. The rheological data were obtained using a Rheometrics Scientific Inc., ARES rheometer. Small strain (10%) oscillatory measurements across a frequency range of 0.03–95 rad/s were made at 190 °C under a nitrogen blanket. The resulting complex viscosity versus frequency data was fitted using the modified Carreau–Yasuda (CY) empirical model [41,42] to obtain the zero shear viscosity (η_0). The molecular weight,

Table 1
Rheology, density, molecular weight and its distribution, and comonomer short chain branch content in LLDPE resinsbased on ethylene/1-butene ('B'), ethylene/1-hexene ('H') and ethylene/1-octene ('O') [28]

Property	Resin 'B'	Resin 'H'	Resin 'O'
MI (g/10 min)[a]	1.09	1.01	1.02
Density (g/cm^3)[b]	0.918	0.918	0.917
Total mol% [X]	2.95	2.47	2.56
η_0 (Pa s)	7.24E3	7.26E3	7.13E3
M_w (kg/mol)	99.0	98.1	97.9
M_n (kg/mol)	44.2	44.2	43.2
M_w/M_n	2.24	2.22	2.27

[a] ASTM D1238.
[b] ASTM D1505.

and the molecular weight distribution were determined by gel permeation chromatography (GPC). Nuclear magnetic resonance (NMR) was utilized to determine the amount of comonomer and thus the short chain branching incorporated into the respective copolymers. The experimental procedures of these two techniques are outlined in detail elsewhere [43]. In addition, the comonomer composition distribution across the molecular weight distribution of these three copolymers was determined by a recently developed chemometric technique [44] based on size exclusion chromatography and Fourier transform infrared spectroscopy (SEC–FTIR).

Temperature rising elution fractionation (TREF) was performed on the three resins to determine the homogeneity of incorporation of SCB in the copolymers. This was done by using a triple detector TREF instrument which was assembled using parts retro-fitted into a Waters 150C GPC system. The column (12.55 mm ID and 150 mm in length) was packed with #30 stainless steel shot (Vulcan Blast Shot Technology, Brantfor, Ont., Canada). The oven heater provided programmed cooling and heating in the 35–150 °C range. It was controlled externally via West 4400 set point programmer. Three detectors, viz. a Foxboro infrared (IR) (3.4 nm), a Viscotek 150R viscometer and a PDI 15 and 90-degree dual-angle light scattering detector, were utilized for characterization. The viscometer and the light scattering detector were housed in the same oven while the IR cell was heated separately. Sample solutions were prepared in the carrier solvent, 1,2,4-trichlorobenzene (TCB), at 3 mg/mL. In the experiment, 500 mL of the sample solution was injected onto the column at 150 °C and subsequently cooled to 35 °C at a rate of 0.72 °C/min, to allow slow and complete crystallization. The column was then slowly re-heated to 150 °C at a rate of 1.5 °C/min with a solvent flow rate of 0.5 mL/min, during which the polymer molecules re-dissolved and eluted out into the three detectors. Analysis of the data obtained from the IR detector was done to get normalized weight fraction of the fractionated copolymer as a function of the temperature.

3.3. Film preparation

Blown films were made from each of the three resins under the following conditions: 100 mm (4 in.) die diameter, 1.5 mm die gap, 37.5 mm diameter single-screw extruder ($L/D = 24$, compression ratio 2.2:1), 115 rpm screw speed (ca. 27 kg/h output rate), 2.5:1 blow up ratio (BUR) and barrel and die temperatures set to 190 °C. The freeze line height (FLH) was between 20 and 28 cm and cooling was accomplished with a dual lip air ring using ambient air that had a temperature of ca. 20 °C. Films with different thicknesses (12.5–100 μm or 0.5–4 mil) were produced this way. These conditions are representative of typical commercial scale LLDPE blown film processing according to scaling procedures established previously [45].

In addition to these blown films, unoriented quenched and slow cooled compression molded films were also produced. Preweighed amounts of the copolymer pellets were melted in a mold at 150 °C for 10 min followed by the application of 3000 lb f (ca. 1350 kg f) for 5 min. Quenched (Q) samples were prepared by being removed from the heater plates followed by being placed on a wooden laboratory bench and exposed to ambient conditions. The samples took ca. 5 min to cool to ambient temperature (ca. 20 °C). For the slow cooled (SC) samples, the mold containing the molten film was allowed to remain between the heater plates after the pressure was released. The power to the heater plates was then turned off to allow slow cooling of the films. The samples attained room temperature in ca. 8 h. Both the Q and SC films were ca. 125 μm (5 mil) in thickness.

3.4. Film characterization

The blown films of different thicknesses were tested for their dart impact strength, Spencer impact strength and Elmendorf tear resistance according to ASTM D-1709 (method A), ASTM D-3420 (although a special in-house pendulum was utilized to ensure failures) and ASTM D-1922 standards, respectively, at ambient conditions. In addition, high-speed puncture resistance of the LLDPE copolymers, at a high impact velocity (5.1 m/s), was also investigated. For this test, quenched compression molded and slow cooled plaques of approximately 3.35 mm thickness were employed. The compression molded specimens (corresponding to 'B', 'H' and 'O') were clamped in a circular fixture that is 76 mm in diameter. A 23.76 kg mass tup/dart (13 mm diameter hemispherical end) was dropped on the clamped specimens at an impact velocity of 5.1 m/s (corresponding to a drop height of 1 m). The direction of impact was parallel to the specimen thickness, and the point of impact was at the center of the clamped specimen. The tup/dart was equipped with a load sensor to measure the load response as a function of time, during the impact event. A separate photo sensor provided a measurement of the initial impact velocity. At a given weight of the tup/dart assembly and its impact velocity, the specimen load-deflection data for the impact event was recorded. Total energy (J) to rupture as measured from the load-deflection curve was used to characterize the impact performance. The quantities (energy to rupture) measured from this test are not fixed material properties as they depend on the test specimen size (thickness) and the specific test conditions.

Blown films that were 25 μm in thickness (each from resins based on 1-butene, 1-hexene and 1-octene) in addition to the compression molded films were chosen for the rest of the characterization methods utilized including refractive index measurements, differential scanning calorimetry (DSC) and essential work of fracture analysis. Flat plate wide angle X-ray scattering (WAXS) patterns of the blown films were obtained at ambient conditions using a Philips PW1720 X-ray generator. Four layers of each of the 25 μm (1 mil) thick blown film (based on 1-butene,

1-hexene and 1-octene) were carefully aligned and stacked on the sample holder to obtain sufficient scattering intensity for exposure of the WAXS pattern at 40 kV, 20 mA and 4 h. The sample to imaging plate distance was 5 cm. The X-ray beam was parallel to the normal of the sample plane.

Pin-hole collimated small-angle X-ray scattering (SAXS) profiles of compression molded films were collected at ambient temperature using a Rigaku Ultrax18 rotating anode X-ray generator operated at 40 kV and 60 mA. A pyrolytic graphite monochromator was used to filter out all radiation except the Cu K_α doublet, with an average wavelength of 1.5418 Å. The camera used 200, 100 and 300 nm pinholes for X-ray collimation. Two-dimensional data sets were collected using a molecular metrology 2D multi-wire area detector, located ca. 65 cm from the sample. After azimuthal averaging, the raw data was corrected for detector noise, absorption, and background noise. The data were then placed on an absolute scale using a type 2 glassy carbon sample 1.07 mm thickness, previously calibrated at the advanced photon source at the Argonne National Laboratory, as a secondary standard. All the SAXS profiles presented have been masked in the low scattering vector region where the beam stop influenced the profiles.

Refractive index measurements were conducted at ambient conditions on all the compression molded films and the 25 μm (1 mil) thick blown films using a Metricon Prism coupler Model 2010 along the three coordinates. Measurements in the normal (ND), machine (MD) and transverse direction (TD) were recorded. An average of 3–5 measurements was reported in each direction. Thermal behavior was investigated on a Seiko SSC/5200 DSC. The heating and cooling traces were recorded at 20 °C/min in a nitrogen-purged atmosphere to study the melting and crystallization of these samples. Small angle light scattering (SALS) patterns in the *Hν* configuration were recorded at ambient conditions by utilizing a He–Ne laser at 633 nm. The sample to imaging plate distance was 11 cm.

Crystalline, amorphous and interfacial contents in compression molded films were estimated by analyzing the free induction decay (FID) data obtained from NMR (method described below), although Alamo et al. [26] and Mandelkern et al. [46,47] have utilized a different method involving analysis of Raman spectra on LLDPEs based on 1-butene, 1-hexene and 1-octene. In the present study, all NMR measurements on compression molded films were made using an Auburn IMR analyzer operating at 20 MHz. Morphological analysis was accomplished by fitting the free induction decay (FID) to a three-component model, viz. crystalline, amorphous and interfacial. The data was obtained using a 90° pulse (2 ms), 1 s pulse delay (which was much greater than five times T_1) and a 17 ms dead time to eliminate signal contamination from the probe ring down. Each FID consisted of 300 points, where each data point was sampled every 1 ms, with 160 transients acquired to improve signal-to-noise. The model utilized to fit the data was based on the procedure suggested by Kristiansen [48]. The signal intensity versus time for hydrogen nuclei located in the crystalline domain is represented by [49,50]:

$$P(t) = \sqrt{\frac{\pi}{6}}\exp\left[-\frac{1}{2}\beta^2 t^2\right]\left\{\frac{\cos\alpha t}{\sqrt{\alpha t}}C\left[\sqrt{\frac{6\alpha t}{\pi}}\right] + \frac{\sin\alpha t}{\sqrt{\alpha t}}S\left[\sqrt{\frac{6\alpha t}{\pi}}\right]\right\} \quad (6)$$

where α is related to the hydrogen–hydrogen distance and β is related to the width of Gaussian broadening. Since, α and β are associated with the crystalline domain, and more specifically a function of the hydrogen–hydrogen distance, these two parameters are expected to be constant. Therefore, a series of ten resins with densities from 0.918 to 0.960 were analyzed. The values found for α and β did not vary much and average values obtained were: $\alpha = 1.070e+05$, $\beta = 72{,}940$. These were used in all the fits reported in this study. The two functions $C[x]$ and $S[x]$ are also referred as Fresnell functions.

The best fit of the signal intensity–time relationship for the hydrogen nuclei located in the non-crystalline domains, viz. interfacial and amorphous, can be expressed as the Weilbullian function:

$$I(t) = A\exp\left\{-\frac{(t)^{\mathrm{d}}}{T_2}\right\} \quad (7)$$

where two separate sets of values of the pre-exponential factor, A, spin–spin relaxation time, T_2, and the Weilbullian factor, d, were utilized for amorphous and interfacial domains, respectively. The three equations were then solved simultaneously by putting the FID data into an Excel spreadsheet and using Microsoft Solver to find the best least squared fit between the experimental data and the model.

Tensile stress–strain curves were recorded at 1 m/s on a specialized MTS system 810. The servohydraulic actuator was operated in displacement control. The force transducer (Kistler 9712B50) was mounted directly to the crosshead. The force signal was amplified with a Kistler 5010B and acquired with a Nicolet Integra oscilloscope at data acquisition rates of 10–40 kHz, depending on specimen type. The specimen geometry utilized for tensile tests was rectangular, 75×17 mm^2. The distance between the jaws of the tensile tester was 10 mm. For the DENT mode, specimens of 25.4×25.4 mm^2 (1×1 in.^{2}) with ligament lengths of 1, 2 and 3 mm were tested at 1 m/s. It is noted that for blown films, the specimens deformed in the MD direction are representative of the measurement in the TD as the crack propagates in the TD. Likewise, the samples deformed in the TD are representative of the measurements in the MD. Thus, the EWF results for blown films are reported corresponding to the direction of the propagation of the crack. For a thorough regressional analysis, at least five specimens were tested at each ligament length. Prior to

testing, the specimens were weighed to compute the average thickness of the film in the ligament region. Individual force–displacement curves were integrated by a computer program to calculate the total fracture energy. This was then normalized by the area of the ligament to provide the specific fracture energy (w_f) and then plotted against the ligament length (l). Regression analysis of this data was performed to obtain the values of the intercept which equals the essential work of fracture, w_e.

4. Results and discussion

As can be seen in Table 1, the three copolymers ('B', 'H' and 'O') are essentially identical in their basic molecular and rheological characteristics. These three resins have a very similar melt flow index (1.01–1.09 g/10 min) and density (0.917–0.918 g/cm^3). The number average (M_n) and weight average molecular weight (M_w) obtained from the GPC are nearly identical (43.2–44.2 and 97.9–99 kg/mol, respectively). The GPC curves for each of the three resins, as shown in Fig. 2 are also comparable. This behavior is further supported by very similar zero shear rate viscosity values (7.13–7.26 kPa s). The polydispersity (2.22–2.27), that reflects the breadth of the molecular weight distribution, and the total comonomer content (2.47–2.95 mol%), as obtained by NMR, is also very similar for each of these three resins. The NMR data also indicate the presence of small levels of ethyl branches in the 'H' and 'O' resin (0.12 and 0.15 mol%, respectively). This is due to the generation of a small level of 'in situ' ethyl branches that are indistinguishable from the ethyl branches introduced by 1-butene in the copolymerization of 'B' copolymer. For the 'H' and 'O' resins, these ethyl branches were detected by NMR in addition to the butyl and hexyl branches, respectively. Thus, the total mol% reported in Table 1 reflects the total amount of short chain branches (including the very small amount of ethyl branches in addition to the butyl or hexyl branches, respectively, for the 'H' and 'O' resins). Nevertheless, the total comononer content ([X] mol%) required to make a 0.918 g/cm^3 density is somewhat higher for the 1-butene copolymer than those based on 1-hexene and 1-octene. The short chain branching distribution data is plotted in Fig. 2 (secondary ordinate axis). The number of short chain branches/1000 C atoms in each of three resins is essentially uniform (9–11/1000 C) across the width of the molecular weight distribution. Despite some scatter at the low and high-end of the molecular weight distribution that is attributed to higher error in the measurements [44], the three copolymer resins indicate a similar SCBD. Another parameter that indicates the uniformity of the distribution of short chain branches across the MWD is the % relative monomer dispersity (%RMD) index, as determined by solution NMR [51,52]. RMD is the tendency of the comonomer units to be either 'isolated' (%RMD = 100) or 'clustered' (%RMD < 100). The values of the three resins utilized in this study are essentially the same, viz. 99.1, 99.7 and 99.3% for 'B', 'H' and 'O', respectively.

The information from the chemometric technique to determine the SCBD (as reported in Fig. 2) does not indicate the distribution of the short chain branches along a given polymer chain. To ascertain any difference in this distribution for the three copolymers, TREF was performed on each of the LLDPE resins. These results are provided in Fig. 3. All three resins ('B', 'H' and 'O') possess the general comonomer distribution profile characteristic of the resins produced by single site metallocene catalysts [53,54]. In the Ziegler–Natta catalyzed LLDPE resins, a low temperature peak (between 45 and 55 °C) that is due to the elution of a soluble fraction heavily concentrated with comonomers and

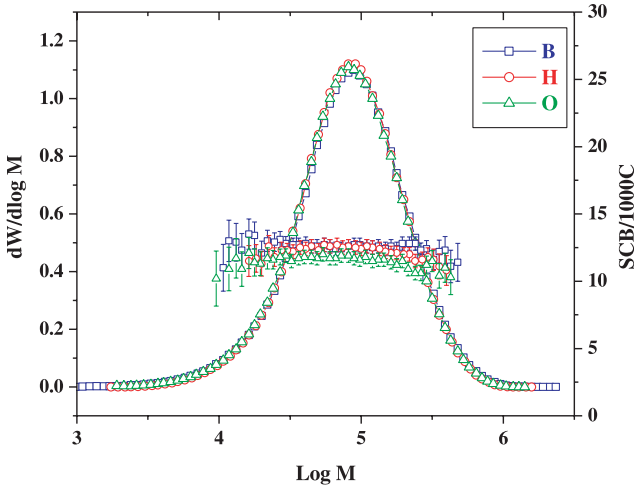

Fig. 2. Molecular weight distribution and the number of short chain branches (corresponding to each resin) per 1000 carbon atoms of the backbone of the three LLDPE resins (indicated on the secondary ordinate axis).

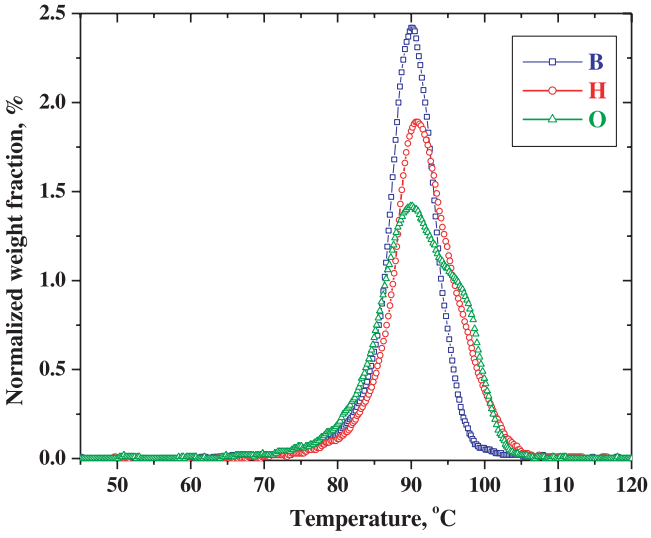

Fig. 3. TREF profiles of the three LLDPE resins based on 1-butene, 1-hexene and 1-octene.

a broad peak in the 55–80 °C range that is due to the elution of 'branched' fraction made up of polymer molecules of various comonomer contents are also observed [55]. However, the absence of the low temperature peaks (in the range of 45–80 °C) in the TREF profiles of metallocene catalyzed LLDPE resins utilized in this study indicate a homogenous incorporation of the short chain comonomer in the linear ethylene backbone as compared to resins synthesized by Ziegler–Natta catalysts. A closer inspection of the three profiles in Fig. 3 indicates some differences that are most likely attributable to some level of difference in the SCB distribution (along a given polymer chain) among the three copolymers utilized in this study. These differences show that resin 'B' has the most homogeneous crystallizability/solubility behavior in comparison to 'H' and 'O'. These differences were primarily manifested in the 'second heating' DSC results on blown and compression molded films (results discussed in detail later, Figs. 8(b) and 9(b)), where the presence of a low temperature shoulder on the melting endotherms of 'H' and 'O' in comparison to 'B' was observed. This difference in the second melting DSC behavior of 'H' and 'O' in comparison to 'B' could arise from the slightly more homogenous distribution of SCB (along the ethylene backbone) in 'B' than 'H' and 'O', as indicated by TREF profiles. However, the SCBD data in Fig. 2 and the near 100% RMD values of the three resins indicate that the overall or average SCB distribution across the MWD is in fact very similar for all three copolymers. Hence, we believe that the magnitude of any differences that may be observed in physical properties (discussed later) cannot simply be attributed to this difference in the TREF profiles.

The refractive index data on compression molded and 25 μm (1 mil) thick blown films is listed in Table 2. As can be observed, within a given series (be it quenched, slow cooled or blown) the average refractive index for the three resins is essentially the same. As expected, the average refractive indices of the slow cooled films are somewhat higher than the corresponding quenched and blown films. For the blown films, the refractive index was observed to be slightly higher in the MD than that in TD, as might also be expected. The difference in the refractive indices in the MD and TD directions, respectively, $n_{MD}-n_{TD}$, gives the in-plane birefringence, Δn. These are listed as well in the extreme right in Table 2. The small values of Δn do not indicate a high level of orientation along the MD (in comparison to that in TD) in these films. The out-of-plane birefringence, $n_{MD}-n_{ND}$, is 0.0013, 0.0011 and 0.0015 for 'B', 'H' and 'O' blown films, respectively. These values are comparable to the in-plane birefringence, thereby indicating a slight uniaxial orientation for these blown films. The WAXS patterns taken with the beam parallel to the sample film normal are shown in Fig. 4. The intensities of the (1 1 0) and (2 0 0) reflections show some azimuthal dependence, as expected. In particular, the (200) reflections are slightly lower in intensity at the equator than that at the meridian, thereby indicating a low *a*-axis orientation along the MD. This is a common observation for polyethylene blown films produced at low stress levels. As expected, the (110) plane reflections, on the other hand, have a relatively lower meridianal intensity than that observed equatorially.

Returning to the refractive index data in Table 2, the density of the films from the average refractive index was calculated by the following relationship [56]:

$$\rho = \left(\frac{1}{r}\right)\left(\frac{\bar{n}^2-1}{\bar{n}^2+2}\right) \tag{8}$$

where $r=0.3278$. From the density of the samples, the % crystallinity (volume) was computed by the following relationship:

$$\%X_c = \left(\frac{\rho-\rho_a}{\rho_c-\rho_a}\right)\times 100 \tag{9}$$

where ρ is the sample density, ρ_a is the density of 100% amorphous polyethylene and ρ_c is the density of 100% crystalline PE. The values of ρ_a and ρ_c were taken as 0.85 and 1 g/cm^3 [57], respectively. The density and $\%X_c$ for all the LLDPE films are listed in Table 2. For the samples in a given series (be it quenched, slow cooled or blown), the films (based on 'B', 'H' and 'O') had essentially the same density and consequently $\%X_c$ within limits of experimental error. This is in agreement with the results reported by Alizadeh et al. [25] (as pointed out earlier), who observed a very comparable degree of crystallinity for compression

Table 2
Percentage crystallinity of LLDPE compression molded and blown films as calculated by refractive index measurements

Material	$n_{(ND)}$	$n_{(TD)}$	$n_{(MD)}$	$\bar{n}$	ρ (g/cm^3)	% X_c (vol.)	Δn ($n_{MD}-n_{TD}$)
B–Q	1.5142	1.5148	1.5150	1.5145	0.9192	44.3±0.4	–
H–Q	1.5141	1.5141	1.5143	1.5141	0.9186	43.9±0.1	–
O–Q	1.5135	1.5147	1.5152	1.5141	0.9186	43.9±0.9	–
B–SC	1.5156	1.5167	1.5165	1.5162	0.9216	46.0±0.6	–
H–SC	1.5147	1.5168	1.5165	1.5158	0.9210	45.6±1.2	–
O–SC	1.5136	1.5161	1.5159	1.5149	0.9197	44.6±1.4	–
B-blown	1.5127	1.5132	1.5140	1.5130	0.9169	42.7±0.7	0.0008
H-blown	1.5129	1.5128	1.5140	1.5129	0.9167	42.5±0.7	0.0012
O-blown	1.5122	1.5129	1.5137	1.5126	0.9162	42.2±0.8	0.0009

Note the birefringence (Δn) of the blown films as computed by the difference in the refractive indices in the MD and TD directions.

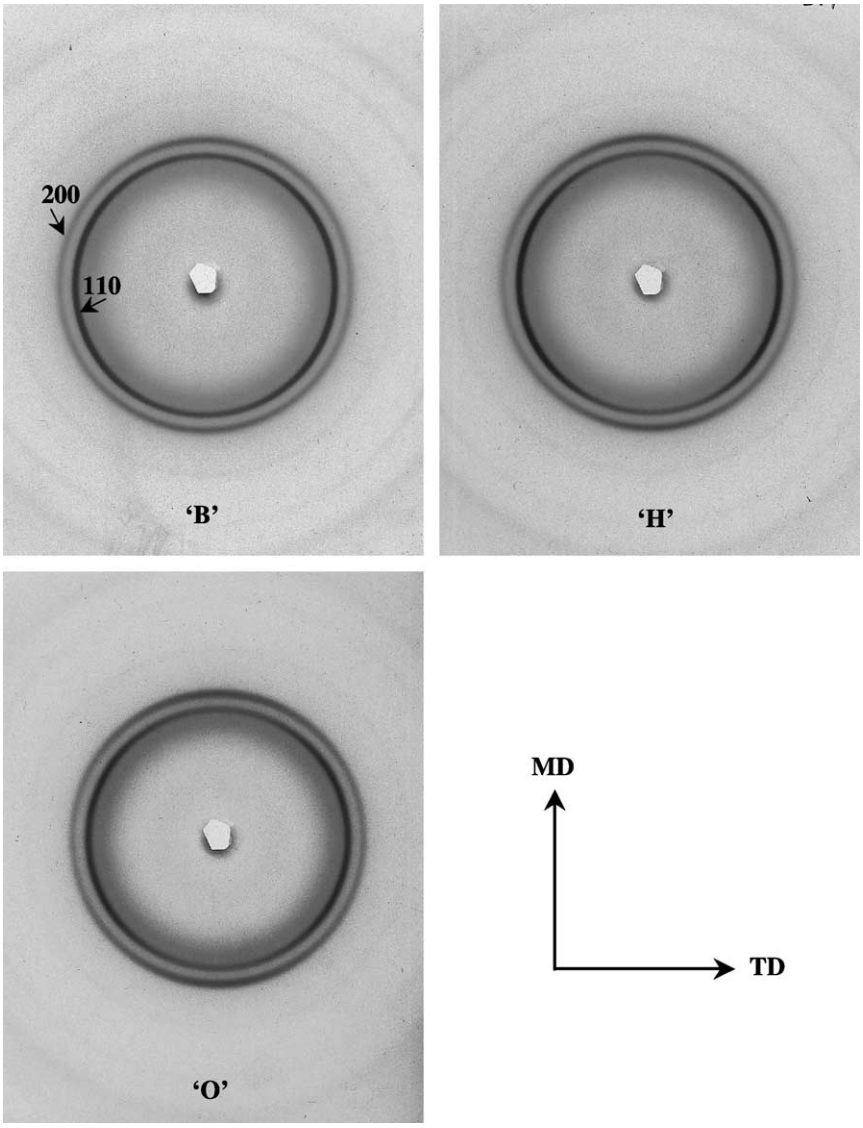

Fig. 4. Flat plate WAXS patterns of the 25 μm thick blown films.

molded quenched LLDPE films based on 1-butene, 1-pentene, 1-hexene and 1-octene at a given mol% of the short chain branch comonomer. Their work did not support the notion that any of the short chain branches are included in the crystalline lattice. In the present study, the density and consequently the $\%X_c$ of the blown and quenched films are lower than the slow cooled samples, as expected.

The lamellar scale lengths in the quenched and slow cooled compression molded films are indicated by SAXS results in Fig. 5. As can be seen, within a given series, the scattering patterns are essentially identical for 'B', 'H' and 'O'. It is clear that the differences in TREF profiles in Fig. 3 do not affect the SAXS behavior on the lamellar scale for both the series investigated (compression molded quenched and slow cooled). As expected, the long period is larger in slow cooled films (223 Å) than that in quenched films (205 Å). In addition, the results from the free induction decay NMR experiments, that gives information on the

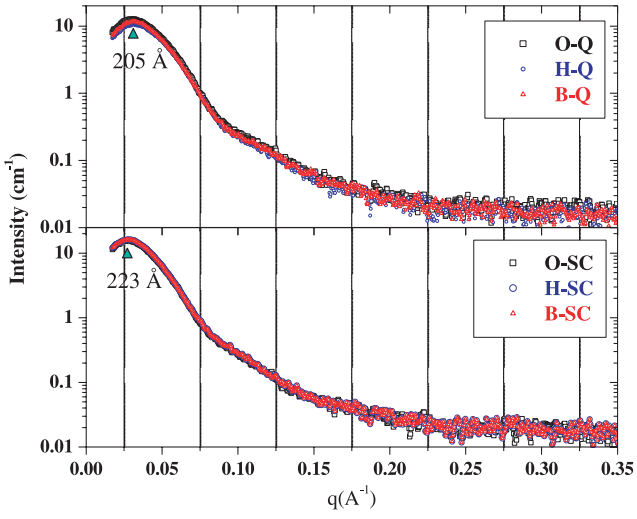

Fig. 5. Small angle X-ray scattering on compression molded films.

relative contents of 'rigid' (crystalline), 'intermediate' (interfacial) and 'mobile or liquid-like' (amorphous) phases indicated that the content of these phases was very similar for 'B', 'H' and 'O' within a given series in the compression molded samples (Fig. 6). For the compression molded quenched samples, the weight fractions of crystalline, interfacial and amorphous domains are ca. 59.5, 29.8 and 11.3%, respectively, in 'B', 'H' and 'O' films, while the respective values for the compression molded slow cooled are 63.1, 24.5 and 12.7%. The calculated crystalline content in the slow cooled films is larger than for the quenched films, as expected. However, the interfacial content in the slow cooled films is slightly less than that in the quenched films, although the amorphous content is very similar in both the compression molded series. In general, the values of crystallinity obtained from free induction decay NMR tends to be higher than those obtained from DSC. This is due to the fact that taut tie molecules can also contribute to the 'rigid' phase. Very recently, Yoon et al. [58] utilized SAXS and solid-state NMR method (rotor-encoded rotational echo double resonance technique) to investigate the structure of metallocene catalyzed LLDPEs as a function of comonomer type (1-butene, 1-hexene and 1-octene) and content. They also did not observe any structural differences in their series of 'B', 'H' and 'O' materials investigated that had a ca. 3 mol% comonomer content.

Returning to the present study, larger scale lengths at the micro level for our materials were characterized by SALS. The spherulitic scale lengths in the compression molded quenched and slow cooled films are indicated by the *Hv* SALS in Fig. 7. As can be seen, the SALS patterns (within a given series, be it quenched or slow cooled), are similar for the 'B', 'H' and 'O'. These 'four-lobed' patterns are characteristic of a spherulitic morphology. However, when comparing the patterns of the slow cooled with that of the quenched films, it appears that the slow cooled films have

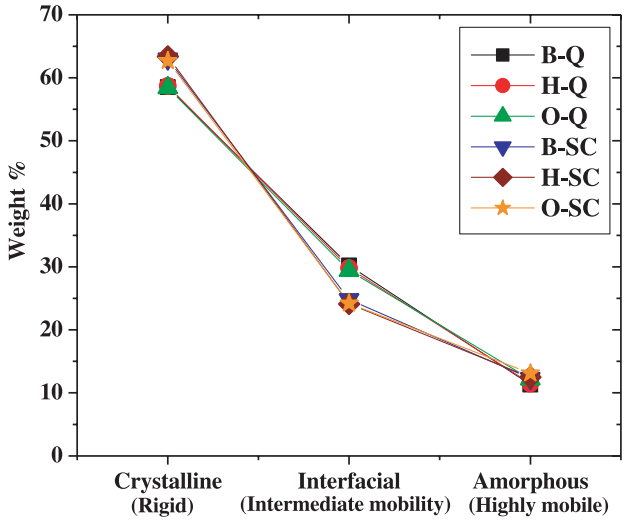

Fig. 6. Crystalline, interfacial and amorphous contents in compression molded films as determined by free induction decay NMR.

larger but less well-defined spherulitic structures than the quenched films. This was also supported by the surface analysis of these films by scanning electron microscopy (SEM) (results not shown here). The SALS patterns in the *Hv* configuration can be utilized to calculate the average size of the spherulites by use of the following relationship [59–61]:

$$\frac{4\pi R}{\lambda_m}\sin\left(\frac{\theta_{max}}{2}\right) = 4.13 \tag{10}$$

where R, is the radius of the spherulites, λ_m is the wavelength in the scattering medium and θ_{max} is the angle of intensity maxima in one of the lobes of the *Hv* pattern. The calculated diameter for the quenched films was in the range of 2.9–3.6 μm (B–Q: 3.3 μm, H–Q: 2.9 μm and O–Q: 3.6 μm) whereas the slow cooled films were in the range of 3.8–4.2 μm (B–SC: 3.8 μm, H–SC: 4.2 μm and O–SC: 4.2 μm). As expected, the size of the spherulites in the slow cooled films is larger than that in quenched films. Furthermore, the SEM analysis on these films indicated a broad distribution of sizes (data not shown).

The first and second DSC heating–cooling profiles of the blown films are shown in Fig. 7(a) and (b), respectively. The first heating (Fig. 8(a)) is extremely comparable for each of the three, 'B', 'H' and 'O' blown films, with melting transition peaks in the range of 117–119 °C. The first cooling curves indicate a lower temperature primary crystallization exotherm peak for 'B' (93 °C) than the 'H' (95.5 °C), which in turn is slightly lower than 'O' (96.5 °C). It might be postulated that a lower primary crystallization temperature peak (higher effective degree of undercooling) indicates crystallization of relatively smaller-sized crystals as compared to the sample that crystallized at a higher temperature. The slightly smaller-sized lamellar crystals should therefore begin to melt at a lower temperature. This is confirmed by the endotherm peak positions in the second heating cycles, where 'B' shows the peak endotherm at 116.5 °C whereas 'H' and 'O' show the second melting endotherm peaks at 117.5 °C. The second heating profiles are shown in Fig. 8(b). A distinct 'shoulder' in the second cycle melting endotherm at 109–113 °C for the 'H' and 'O' films (Fig. 8(b)) can be clearly seen in comparison to the 'B' film, which does not show a distinct shoulder. This difference in the second melting DSC behavior of 'H' and 'O' in comparison to 'B' could arise from the more interchain homogeneity of SCB in 'B' than 'H' and 'O', as indicated by TREF profiles in Fig. 3. Another noticeable and identical feature in the first and second cooling curves is the presence of a small exotherm transition at 63 °C for each of the three films within a given series, be it blown, quenched or slow cooled. This secondary crystallization is postulated to lead to the formation of a second population of lamellar crystals that are thinner than those formed during the primary crystallization process at higher temperatures.

The DSC results of the compression molded films are

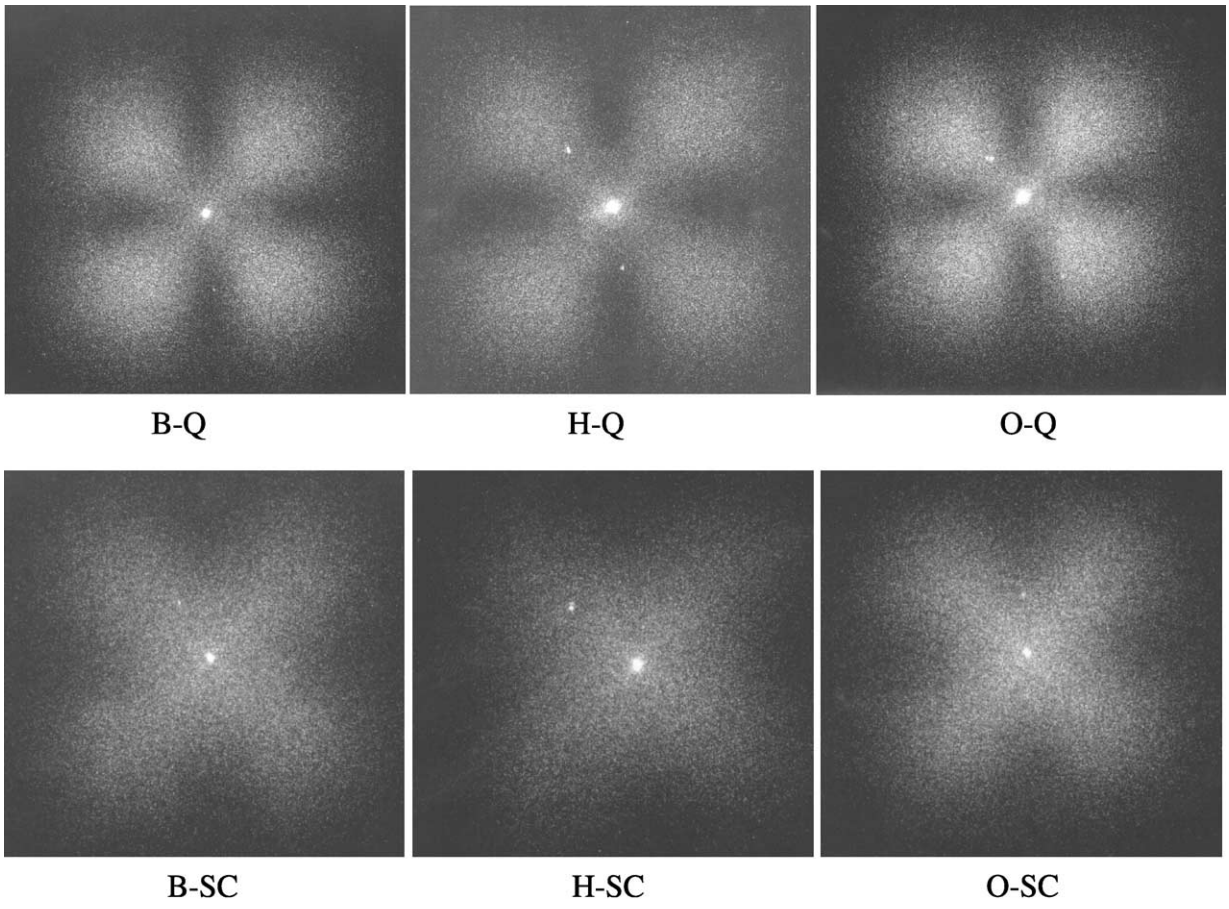

Fig. 7. Small angle light scattering results in the *Hν* configuration on compression molded films.

shown in Fig. 9, where only the heating curves are shown. Based on the first heating curves (Fig. 9(a)), the melting peaks of the quenched and slow cooled films are in the range of 115–117 °C. Only the slow cooled films of 'H' and 'O' show a slightly broader melting endotherm than that of 'B'. These samples were left in the insulated DSC chamber and allowed to cool down to room temperature in about 2 h after which they were heated again and the corresponding second heating curves were recorded (Fig. 9(b)). As can be seen, a behavior similar to what was observed for the blown films is noted. Specifically, the presence of a 'shoulder' on the melting endotherms of 'H' and 'O' (for both quenched and slow cooled) is much more distinct and marked as these samples were cooled very slowly after the first melting (as against a cooling rate of 20 °C/min for the blown films). As stated earlier, the slightly broader first melting endotherms of 'H' and 'O' than 'B' and the difference in the second melting DSC behavior of 'H' and 'O' in comparison to 'B' could arise from the slightly more homogenous distribution of SCB (along the ethylene backbone) in 'B' than 'H' and 'O', as indicated by TREF profiles in Fig. 3. Nevertheless, it can be said that the thermal behavior based on the first heating responses of these films 'B', 'H' and 'O' (be it quenched or blown) are very similar. In the compression molded slow cooled films, whether the slightly broader first melting endotherms of 'H' and 'O' play a role in governing the mechanical properties at slow deformation rates of these films will become clear in the following discussion.

The tensile properties of the 25 μm thick blown films and compression molded films that were measured at slow draw rates, ca. 0.0004–0.008 m/s, (25–510 mm/min) are shown in Fig. 10. The yield and breaking strength are essentially the same for the films based on 'B', 'H' and 'O' in each direction (MD or TD). For the LLDPE blown films, due to preferential orientation of the lamellar crystals, the TD modulus tends to be higher than the MD modulus [13]. However, for the films investigated here, the low levels of orientation translates to the modulus being only marginally higher along the TD. Likewise, the tensile properties of the compression molded films (Fig. 10(b)) at conventional draw rates indicate very comparable yield and breaking strengths for films based on 'B', 'H' and 'O', within a given series. Within the limits of error, the tensile modulus is also very similar for films based on three resins in each series. These results clearly indicate that the slight differences in the TREF profiles in Fig. 3 and differences in first melting DSC profiles of compression molded slow cooled films really do not play any role in governing the mechanical properties when obtained at slow deformation rates (up to 0.008 m/s).

To ascertain any differences in the tensile properties at

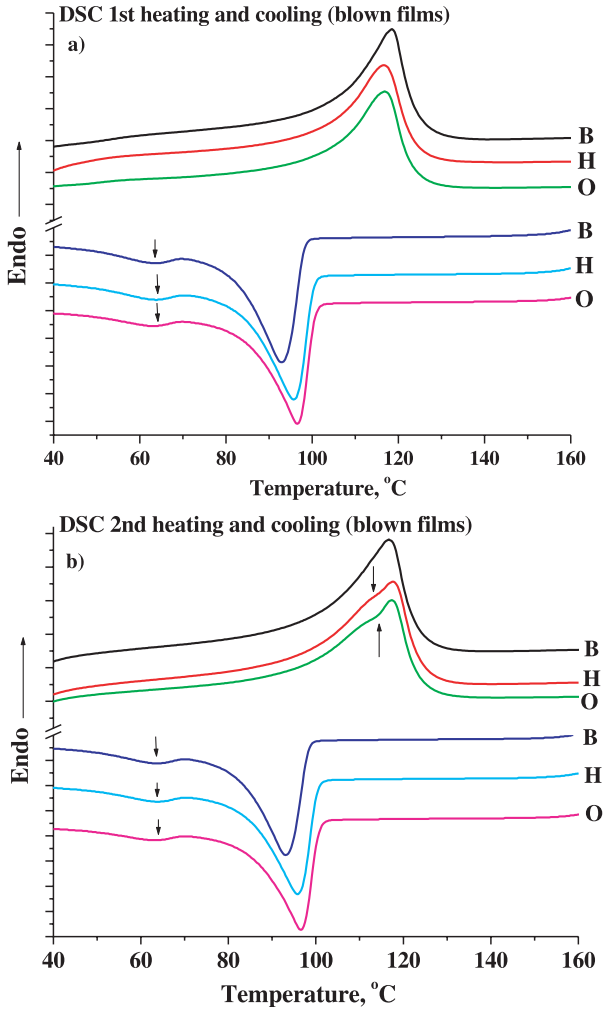

Fig. 8. DSC melting and cooling curves of blown LLDPE films. The (a) first and (b) second heating–cooling cycles measured at 20 °C/min are shown.

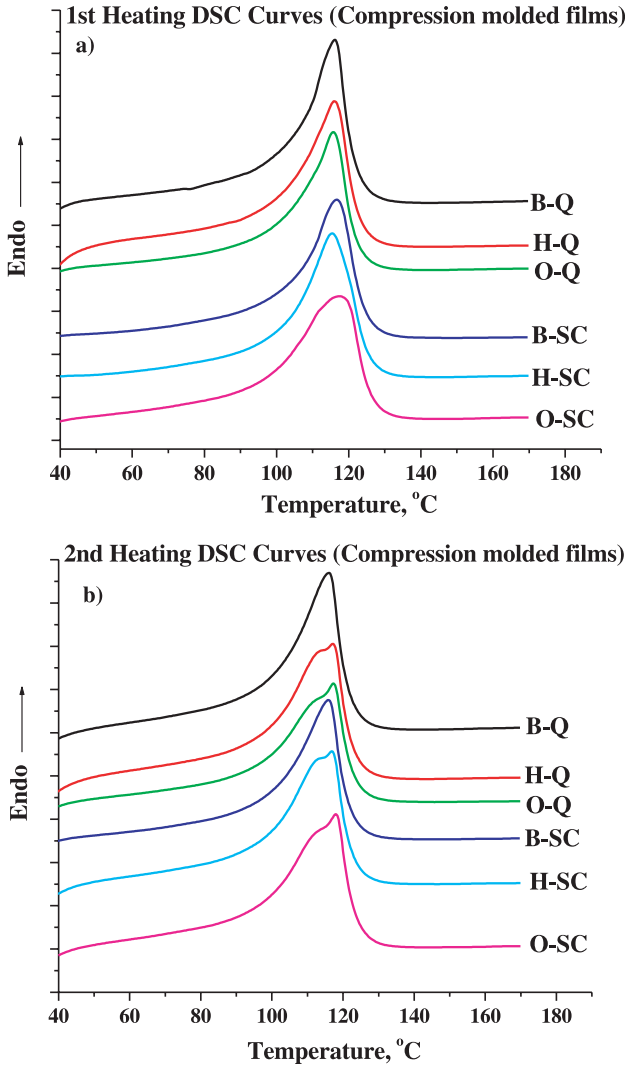

Fig. 9. DSC melting endotherms of compression molded LLDPE films. The (a) first and (b) second heating curves measured at 20 °C/min are shown.

higher deformation rates, the stress strain behavior was measured at a higher deformation rate of 1 m/s (about two orders of magnitude higher than before). These results are shown in Fig. 11(a) and (b) for 25 μm thick blown and compression molded films. Due to the extremely high rate of data acquisition, the 'ringing' characteristics of the load path's mechanical elements (primarily the load cell/grip assembly) appear as oscillations in the 'yield' region of the curves. However, the yield strength values of both the blown and compression molded films are readily distinguished, and all fall in the range of 17–20 MPa. The 'H' and 'O' blown films also show a higher breaking strain than that for corresponding 'B' films (Fig. 11(a)). Likewise, B–Q and B–SC underwent failure before yielding or plastic drawing could take place whereas, with the exception of the 'O–SC', the compression molded 'H' and 'O' materials yield, draw and undergo significant post 'natural draw ratio' deformation before failure (Fig. 11(b)). A noticeable trend was observed in the breaking strengths. The breaking strength of the 1-butene based films ('B') is distinctly lower than that for the 1-hexene ('H') and 1-octene ('O') based films, regardless of film type (quenched, slow cooled or blown). For the blown films, the 'B' films have a breaking strength of ca. 21–24 MPa as compared to that of 31–36 MPa for 'H' and 'O' films. In either direction (MD or TD) the 'H' and 'O' films also show distinctly greater strain hardening when compared to the 'B' films, and this accounts for the higher values of the breaking strengths. Similarly, strain hardening can be observed in the 'H' and 'O' compression molded films. The quenched and slow cooled films of 'B' do not undergo any strain hardening and display much lower breaking strengths (6–10 MPa) as compared to the high values of the 'H' and 'O' films (16–26 MPa). Note that when the breaking strengths of the compression molded and blown films corresponding to the same resin are compared, the blown films have superior properties. Comparing the results in Figs. 9 and 10, it can be inferred that the breaking strength of blown films of 'B' is lower than that of 'H' and 'O', an effect that is evident only at high deformation rates.

Further tests conducted on the blown films to measure

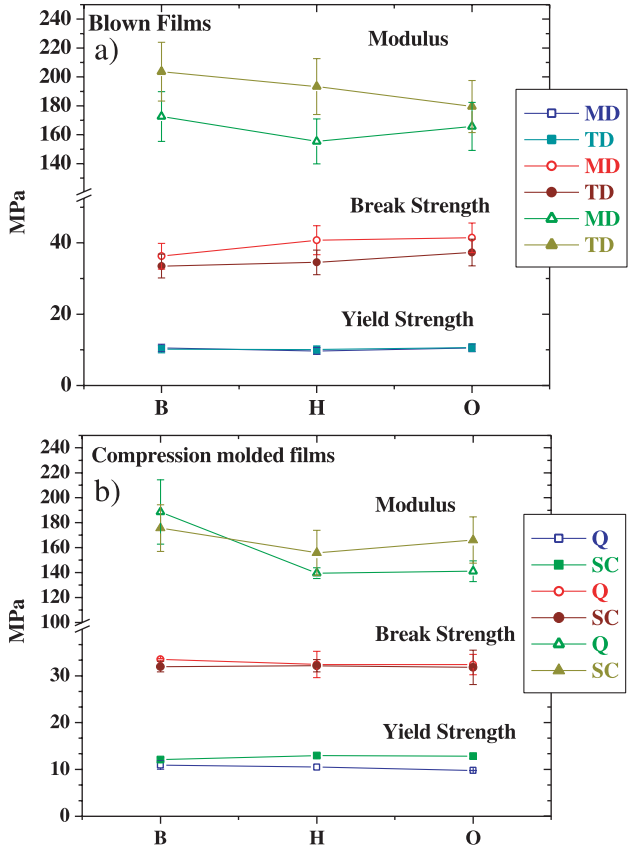

Fig. 10. Tensile properties of (a) 25 μm thick blown films and (b) compression molded films at 0.0004–0.008 m/s (25–510 mm/min).

their dart impact strength, Spencer impact strength and Elmendorf tear properties, where high deformation rates of 0.1–1, 0.1–7 and 0.2–4 m/s, respectively, were utilized, also confirm this behavior. As shown in Fig. 12, the dart impact strength, at any given film gage, of 'B' is significantly lower than that of 'H' and 'O'. During the dart impact testing, some of the films, especially at higher gage, did not rupture at the maximum allowable force corresponding to the falling dart of 1400 g. Hence, those values are reported as '>1400 g' in Fig. 12. Turning to the results in Fig. 13(a) and (b), it is clearly noted that Elmendorf tear and Spencer impact strength increase with increasing short chain branch length at any given blown film thickness. Furthermore, within samples of the same copolymer type ('B', 'H' or 'O') these properties increase with increasing blown film thickness, as would be expected. Of particular importance is that for any given direction (MD or TD), the Elmendorf tear strength and Spencer impact strength increase in the order: 'O' > 'H' > 'B'. The results of the puncture resistance measurements on compression molded quenched and slow cooled plaques are given in Fig. 14, which again support that the materials based on 1-butene are inferior to those based on 1-hexene and 1-octene. The load-deformation curves are plotted in Fig. 14(a) for the representative samples corresponding to 'B', 'H' and 'O', respectively, in each series (quenched and slow cooled). Five specimens

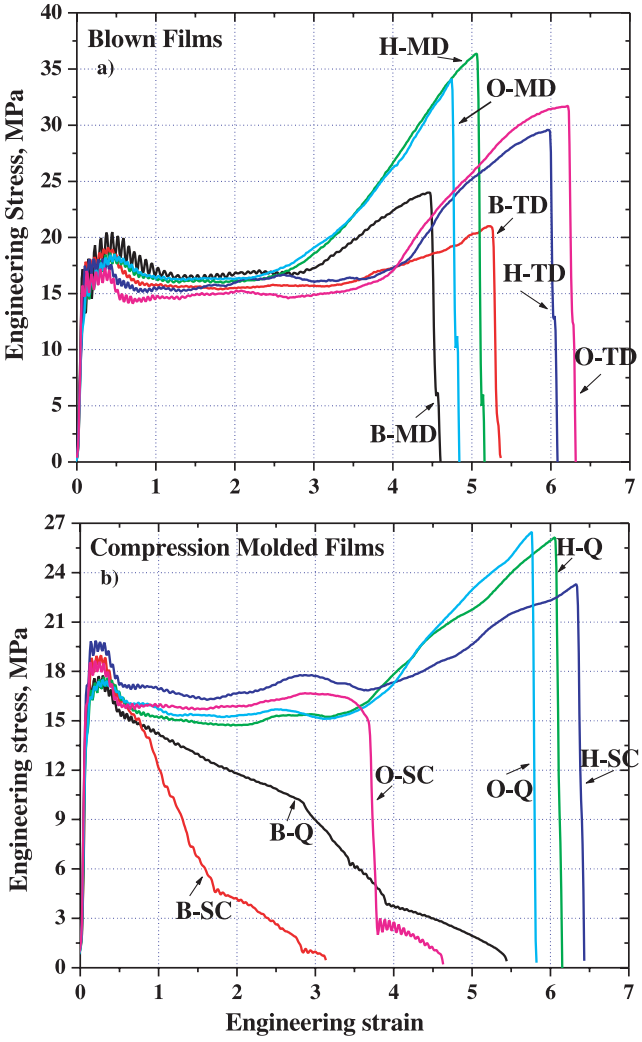

Fig. 11. Engineering stress–strain curves of (a) blown and (b) compression molded films at 1 m/s.

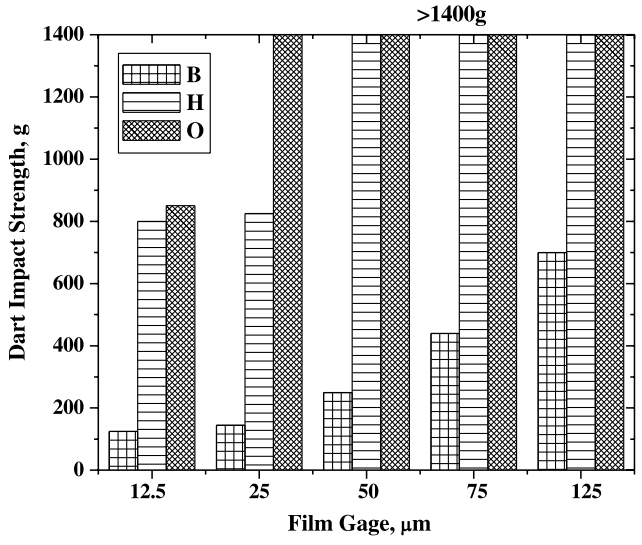

Fig. 12. Dart impact strength of blown films at 0.1–1 m/s.

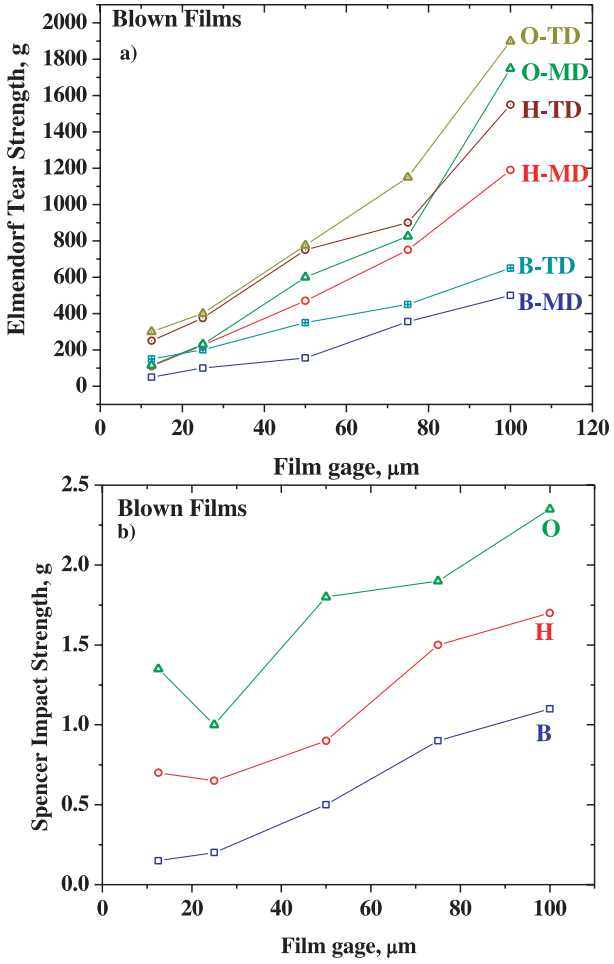

Fig. 13. (a) Elmendorf tear strength at 0.1–7 m/s and (b) Spencer impact strength at 0.2–4 m/s of blown films as a function of the film thickness.

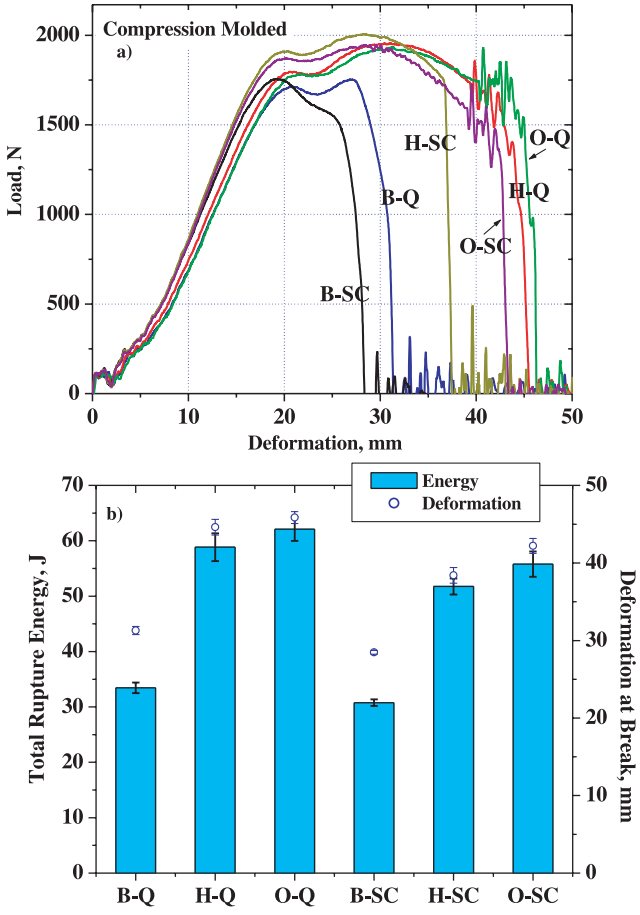

Fig. 14. (a) Sample load–deformation curves corresponding to 'B', 'H' and 'O'; (b) high speed puncture resistance and deformation at break of 'B', 'H' and 'O' materials measured in terms of total rupture energy.

corresponding each to 'B', 'H' and 'O' in each series (quenched and slow cooled) were tested (load-deformation curves of representative specimens shown Fig. 14(a)). The results indicated a good reproducibility for each material type. The average integrated energy to rupture and the deformation to failure are plotted in Fig. 14(b). As can be seen, within a given series, be it quenched and slow cooled, the total deformation to failure (plotted on the secondary axis of Fig. 14(b)), of 'H' and 'O' is higher than that of 'B', indicating an increased ductile failure in 'H' and 'O'. This was also confirmed visually by the fact that the deformed 'H' and 'O' samples had a longer and ductile sleeve (relative to that in 'B') that emanated from the region where the mechanically driven tup exited the sample. This is also reflected as higher total rupture energies for 'H' and 'O' (55–61 J) than 'B' (30–37 J). However, in all these tests, viz. dart impact, Spencer impact and Elmendorf Tear the rate of deformation of the films is not well-defined. In a dart impact measurement, a falling dart ruptures the film held in tension and the equivalent force to rupture is recorded in terms of the mass of the falling dart. In the case of the Spencer impact strength measurements, a piece of film is held in tension and punctured with a hemispherical head attached to a swinging pendulum whereas in Elmendorf tear resistance, the precut film sample is ruptured by a swinging pendulum. In the puncture resistance measurements the sample is held in tension and punctured by a pneumatically driven tup/dart. In either configuration, the deformation rate of the film can be visualized to be a maximum at the initiation (when the pendulum or the ball/dart hits the film) and then decreases thereafter as the crack progresses (as most of the energy carried by the pendulum or the ball/dart has already been spent in overcoming the initial resistance). Thus, the rates of deformation (reported above) are at best estimates and never an exact value, as the deformation process of the samples is not well-controlled.

To characterize the deformation of the films in a more well-defined extensional regime, tear resistance properties were measured by utilizing the essential work of fracture (recall earlier discussion of this methodology). Here, precut films that have a specified ligament length were deformed in a tensile manner at 1 m/s to investigate their tear resistance properties. A typical stress–displacement behavior for the blown film based on resin 'H' is shown for two ligament lengths, viz. 1 and 3 mm in Fig. 15(a) and (b).

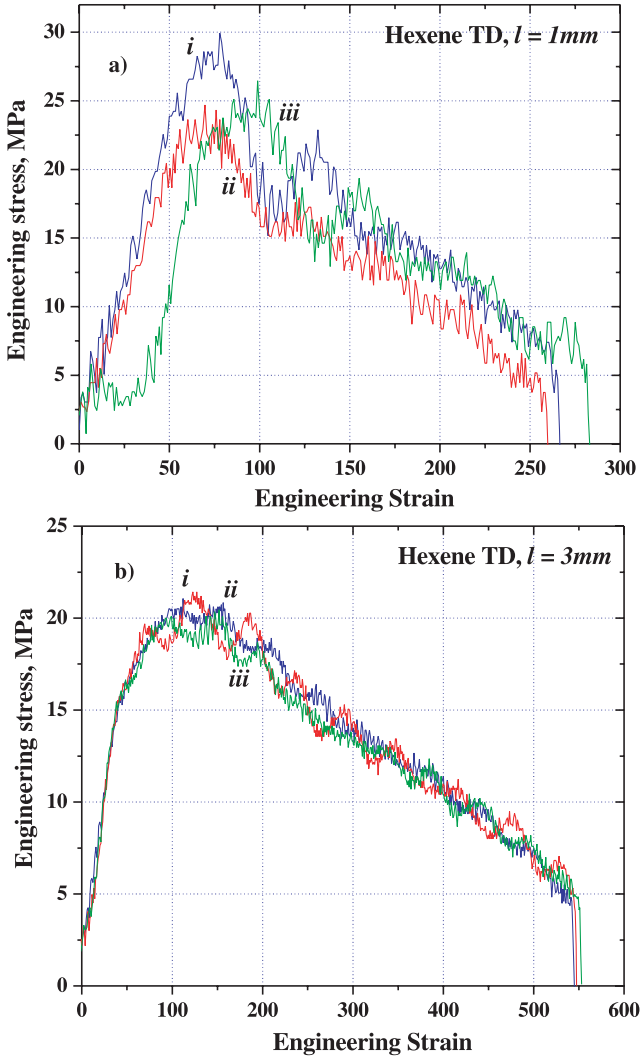

Fig. 15. Sample engineering stress–displacement curves in the double edge notched tensile test (DENT) mode of ethylene/1-hexene blown film in the TD for ligament lengths of (a) 1 mm and (b) 3 mm. Data for four samples (corresponding to each ligament length and marked as *i*, *ii*, *iii* and *iv*) are shown to indicate reproducibility.

Three stress–displacement curves (marked as *i*, *ii* and *iii*) corresponding to three specimens (with the same ligament length) are shown to indicate the reproducibility in the data. The tear specimens satisfy the plane stress conditions [Eqs. (3) and (4) in Section 2] and fail right after the yield and do not undergo any plastic stretching that is characteristic of the samples in a conventional tensile deformation test. Further, the larger ligament length specimens had a larger strain at break. This is due to the fact that at larger ligament lengths, there is more material in the ligament that undergoes deformation in comparison to that in the smaller ligament lengths. However, the yield stress is practically the same at both the ligament lengths, as expected. Stress–displacement curves were obtained in a similar fashion for the 25 μm thick blown films of 'B' and 'O' and all the compression molded films. Based on the procedure outlined in Section 2, the specific fracture energy, obtained by

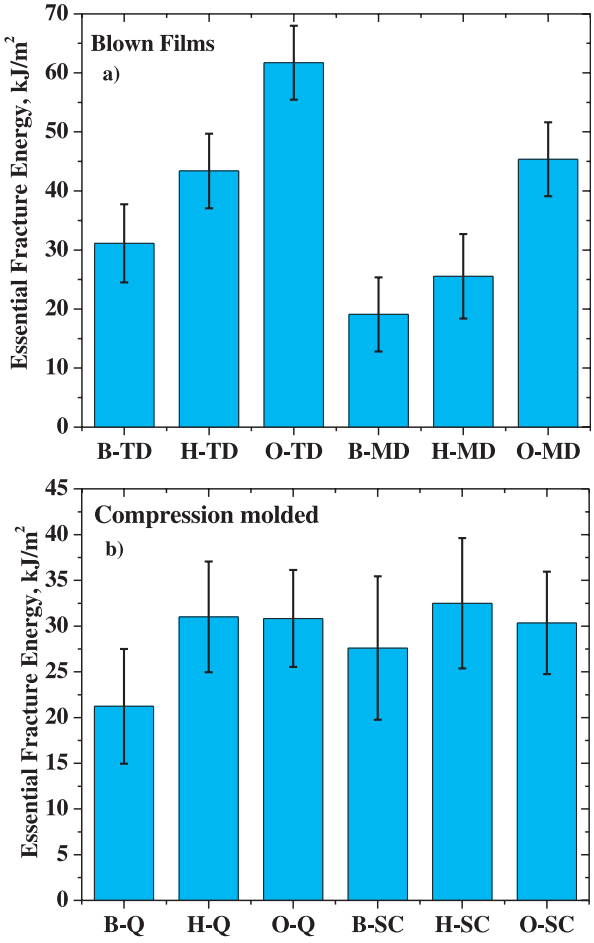

Fig. 16. Essential fracture energy of (a) blown and (b) compression molded LLDPE films.

integrating the stress–strain curve, was fitted by a linear relationship when plotted against the ligament length. The intercepts of these plots, then gave the essential work of fracture. These results are shown in Fig. 16. For the blown films (Fig. 16(a)) in each of the direction (MD or TD), the essential work of fracture is observed to increase with increasing short chain branch length, a result consistent with the impact strength and Elmendorf tear resistance measurements. As stated before, when a blown film specimen is stretched along the MD, the crack propagates along the TD. Therefore, when the specimen is being stretched along the MD, the measured EWF is representative of the TD direction. Consequently, the EWF along the TD is greater than that along the MD. This is consistent with the tear resistance being greater along the TD than along the MD (Fig. 13(a)), which in turn is a manifestation of the preferred lamellar orientation [13,14] (although only slight in this study). For the compression molded quenched films (Fig. 16(b)), the essential work of fracture of films based on 1-butene was also observed to be less than that of the 1-hexene and 1-octene films. However, within the limits of experimental error, the EWF results of the slow cooled films do not indicate a strong dependence on the short chain

branch length. Thus, based on the results discussed so far, it can be inferred that the mechanical properties of the films of the three essentially identical linear low density polyethylene copolymers based on 1-butene, 1-hexene and 1-octene show a dependence on the length of short chain branch only at high rates of deformation. This is summarized in Table 3, where at slower rates of deformation, the mechanical properties were observed to be similar but quite different at higher deformation rates. This is due to the fact that these films are very similar in their molecular, rheological and structural aspects that any effects due to the different short chain lengths (present in small amounts of ca. 2.5–3 mol%) do not get reflected at slower deformation rates. However, at high deformation rates, these effects become prominent such that the mechanical properties of films based on 1-butene were observed to be lower than those based on 1-hexene and 1-octene. Recalling that the primary objective of this study was to further investigate the effect of the length of short chain branch on the physical properties of LLDPEs, the results presented here have shown that the length of the short chain branch does play an important role in influencing the mechanical properties of the LLDPEs in agreement with earlier results [28] and furthermore established that this effect is pronounced only at high rates of deformation.

With regards to the origin of the effect of the difference in short chain branch length on the mechanical properties when measured at high rates of deformation, it seems difficult to attribute this to the amorphous phase in view of the low mole percentage of the branches and the fact that the rheological behavior of at least the melt state shows no significant differences. We did investigate the DMA (dynamic mechanical analysis) behavior of the film materials (data not shown) but did not find any distinct variations between the materials although we admit that the DMA tests were determined in the lower frequency range (0.001–10 Hz). We conjecture that the origin of the effect of the difference in short chain branch length on the mechanical properties is coupled to its influence on the deformation behavior of the crystalline phase. It has been speculated [21,24,62,63] that a short chain branch prevents the formation of crystalline regions in its immediate vicinity leading to an increased probability of the main chain to which it is attached to be incorporated into two different lamellae, thereby establishing that portion of the chain as a bridge or a tie molecule. If this supposition is true, then the enhanced properties, associated with plastic deformation (ductility, toughness, tear resistance, etc.), could be due to an increasing number of tie molecules with increasing molar content of short chain branches. However, this postulate does not explain the EWF results on slow cooled films where the essential work of fracture was not observed to be strongly dependent on the branch length. For the three series of films investigated in this study, viz. the blown, quenched and slow cooled, the latter had the slowest rate of crystallization and hence the highest opportunity to form a more thermodynamically desirable equilibrium structure. Thus, if tie molecule formation is favored at longer branch lengths that consequently result in larger values of strength, then this effect (‘O’ ~ ‘H’ > ‘B’) should be more pronounced in the EWF results on slow cooled in comparison to blown and quenched films. However, this is not the case. Therefore, it is difficult to envision the increased formation of tie molecules with increasing short chain branch length. We, however, postulate that during the process of deformation at high rates (1 m/s), the length of the short chain branch may play an important role when it is pulled into and potentially through the chain folded lamellar regions as they deform. A very simplified schematic of this concept is shown in Fig. 17. The magnitude of the resistance offered by a shorter branch length undergoing deformation through the crystalline regions could be lower than that experienced by a longer branch length. Furthermore, for LLDPEs that have only a few mol% (< 5 mol%) of the short chain branch comonomer, it is possible that this effect would be pronounced at higher rates of deformation. This is because at lower rates (0.0004 m/s) of deformation the polymer chains have a longer time scale to respond to the deformation, and consequently the resistance offered by the branch during deformation may be independent of its length. However, while this explanation is a hypothesis that might explain the observed phenomena, it is yet to be confirmed. Future investigations need to be conducted to gain an in-depth understanding of the mechanism of deformation and their rate dependence at the molecular level.

In the past, some attempts to investigate the slow crack growth in polyethylenes have been conducted, [64–66]

Table 3
Dependence of mechanical properties on deformation rate

Test	Estimated rate of deformation (m/s)	Properties
Stress strain	0.0002–0.008[a]	Very similar
Stress strain	1	Very different
Dart impact	0.1–1	Very different
Elmendorf tear	0.1–0.7	Very different
Spencer impact	0.2–4	Very different
Puncture resistance	5.1	Very different
Tear resistance (EWF)	1	Different

[a] 12–510 mm/min (conventional crosshead speeds).

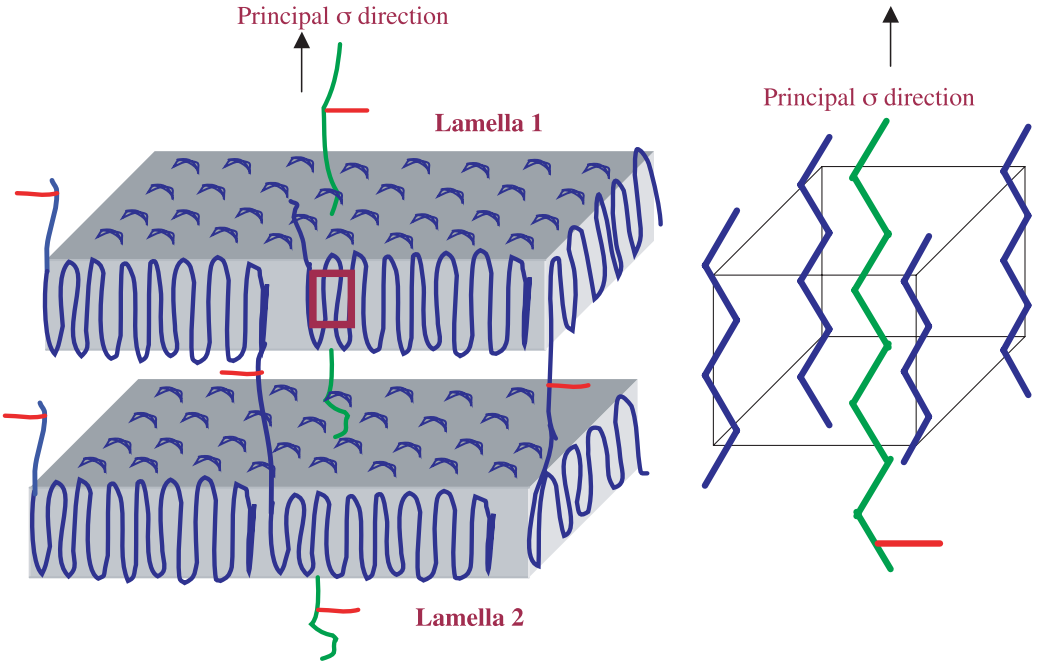

Fig. 17. A schematic showing the possible exclusion of the short chain branches from the chain folded regions leading to the formation of tie molecules. It is hypothesized that the length of the short chain branch plays a role during tensile deformation at extreme strain rates. The dotted square on lamella 1 is enlarged on the right.

however, investigating the specific behavior of the SCB during deformation especially at a higher rate is not trivial as the choice of a suitable experiment that will allow such a characterization is difficult. Another potential way to investigate such behavior at high deformation rates might be by the dynamic modeling of the deformation phenomena that could trace a given SCB as it is pulled through the crystalline regions during the deformation at higher rate. Certainly, as such modeling codes become more predictive, the approach may help to address the distinct differences observed in our study.

5. Summary

Three LLDPE resins synthesized by a single site metallocene catalyst using 1-butene, 1-hexene, and 1-octene as co-monomers were characterized to be essentially identical in terms of their molecular weight and distribution melt rheology, density, crystallinity, and short chain branching content. The resins were also very homogenous with respect to the short chain branch distribution across their MWD, although very slight differences were observed in the TREF profiles of the three resins. Therefore, this sample set allows us to evaluate the exclusive influence exerted by the short chain branch length on the physical properties of the resulting films; many previous attempts by other workers to accomplish the same objective have been confounded by samples that differed substantially in their chemical composition. The physical properties of isotropic compression molded (slow-cooled and quenched) films as well as blown films of the subject LLDPEs were investigated using a variety of tests carried out at widely differing deformation rates. The blown films made from these resins had low levels of equivalent in-plane birefringence and the flat plate WAXS measurements indicated low *a*-axis orientation along the MD (Keller–Machin low stress row structure). Within the compression molded quenched and slow cooled series, the lamellar and spherulitic scale lengths as determined by SAXS and SALS indicated very similar dimensions corresponding to ‘B’, ‘H’ and ‘O’. The blown and compression molded films formed from these resins were also found to be similar to each other (within a given series, be it blown, quenched or slow cooled) in terms of crystallinity, and overall crystallization characteristics, although, slightly broader melting endotherms of ‘H’ and ‘O’ in comparison to ‘B’ were observed in the first melting profiles of compression molded slow cooled films. However, the tensile properties of slow cooled ‘B’, ‘H’ and ‘O’at slow deformation rates (up to 510 mm/min) were very similar, thereby clearly indicating that these slight differences in the TREF behavior and differences in first melting DSC profiles of compression molded slow cooled films really do not play any role in governing the final mechanical properties of the LLDPE films obtained at slower deformation rates (up to 510 mm/min).

At higher deformation rates (1 m/s), however, the breaking strength was observed to increase with increasing short chain branch length for all the samples investigated (blown, quenched and slow cooled). This is consistent with an earlier study [28] utilizing the same polymers and films

investigated here, where the impact and tear strength of blown films based on 1-octene and 1-hexene were found to be considerably better than those of films based on 1-butene. While the deformation rates in the above mentioned tests are quite high, the rates change considerably during the measurement. Therefore, the deformation characteristics of the subject films were also studied in a well-defined and controlled regime by analyzing the essential work of fracture for the blown and compressed films. For the blown films, the essential work of fracture was found to increase systematically with increasing short chain branch length. For the compression molded films, the 1-hexene and 1-octene based films performed better than the 1-butene films. In general, the mechanical properties of 1-octene based systems were somewhat enhanced relative to those based on 1-hexene. However, this is not an all inclusive statement, as the compression molded films of 'O' performed equally to 'H' in high speed tensile (breaking strength at 1 m/s), puncture resistance and EWF tear tests. From these results, it can be concluded that the length of the short chain branch length plays a crucial role in determining the mechanical properties of LLDPE, especially at high deformation rates. It is hypothesized that the magnitude of the resistance offered by a shorter branch length undergoing deformation through the crystalline regions could be lower than that offered by a longer branch length. However, further studies to gain a better understanding of the underlying physical process of deformation need to be conducted.

Acknowledgements

The financial support of the US Army Research Laboratory and US Army Research Office under contract/grant number DAAD19-02-1-0275. Macromolecular Architecture for Performance (MAP) MURI is gratefully acknowledged. The authors would like to thank Chevron Phillips Chemical Company and Procter and Gamble Company for their collaboration and support.

References

[1] Natta GJ. Polym Sci 1959;34:531–49.
[2] Lai S, Knight GW. Proceedings of the 51st annual technical conference. New Orleans, LA, USA: Society of Plastics Engineers; 1993, p. 1188.
[3] Montagna AA, Floyd JC. Hydrocarbon Process, Int Ed 1994;73:57–60.
[4] Benedikt GM, Goodall BL. Metallocene catalyzed polymers—materials, properties, processing and markets. Ont., Canada: ChemTec Publishing; 1999.
[5] Benedikt GM. Metallocene technology in commercial applications. Ont., Canada: ChemTec Publishing; 1998.
[6] Sukhadia AM. J Plast Film Sheeting 1998;14:54–75.
[7] Bubeck RA, Baker HM. Polymer 1982;23:1680–4.
[8] Maddams WF, Preedy JE. J Appl Polym Sci 1978;22:2721–37.
[9] Maddams WF, Preedy JE. J Appl Polym Sci 1978;22:2739–49.
[10] Maddams WF, Preedy JE. J Appl Polym Sci 1978;22:2751–9.
[11] White JL, Cakmak M. Adv Polym Tech 1988;8:27.
[12] Pazur RJ, Prud'homme RE. Macromolecules 1996;29:119–28.
[13] Krishnaswamy RK, Lamborn MJ. Polym Eng Sci 2000;40:2385–96.
[14] Krishnaswamy RK, Sukhadia AM. Polymer 2000;41:9205–17.
[15] Haber A, Kamal MR. Proceedings of the 45th annual technical conference, Los Angeles, CA, USA: Society of Plastics Engineers; 1987; p. 446.
[16] Lee C, Peat I, Wild L, Fernando A. Proceedings of the 46th annual technical conference, Atlanta, GA, USA: Society of Plastics Engineers; 1988; p. 183.
[17] Firdaus V, Tong PP. J Plast Film Sheeting 1992;8:333–40.
[18] Crotty VJ, Firdaus V. Proceedings of the 51st annual technical conference, New Orleans, LA, USA; Society of Plastics Engineers; 1993; p. 210.
[19] Patel RM, Butler TI, Walton KL, Knight GW. Polym Eng Sci 1994;34:1506–14.
[20] Cady LD. Plast Eng 1987;43:25–7.
[21] Liu TM, Baker WE. Polym Eng Sci 1992;32:944–55.
[22] Kim Y-M, Park J-K. J Appl Polym Sci 1996;61:2315–24.
[23] Wolfe AR. Plastics pipes X: Plastics pipeline systems for the millennium, conference papers, Goeteborg, September 14–17, 1998. p. 95–102.
[24] Kale LT, Plumley TA, Patel RM, Redwine OD, Jain P. J Plast Film Sheeting 1995;12:27–39.
[25] Alizadeh A, Richardson L, Xu J, McCartney S, Marand H, Cheung YW, et al. Macromolecules 1999;32:6221–35.
[26] Alamo RG, Viers BD, Mandelkern L. Macromolecules 1993;26:5740–7.
[27] Kennedy MA, Peacock AJ, Failla MD, Lucas JC, Mandelkern L. Macromolecules 1995;28:1407–21.
[28] Sukhadia AM, Welch MB, Krishnaswamy RK, Palackal SJ. Proceedings of the 58th annual technical conference. vol. 2. Orlando, FL, USA: Society of Plastics Engineers; 2000. p. 1578–82.
[29] Ferrer-Balas D, Maspoch ML, Martinez AB, Santana OO. Polymer 2000;42:1697–705.
[30] Chan WYF, Williams JG. Polymer 1994;35:1666–72.
[31] Maspoch ML, Ferrer-Balas D, Gordillo A, Satana OO, Martinez AB. J Appl Polym Sci 1999;73:177–87.
[32] Maspoch ML, Perez-Gamez GA, Sanchez-Soto M, Velasco JI. Polymer 2002;43:4177–83.
[33] Ferrer-Balas D, Maspoch ML, Martinez AB, Ching E, Li RKY, Mai Y-W. Polymer 2001;42:2665–74.
[34] Cotterell B, Reddel JK. Int J Fract 1977;13:267–77.
[35] Broberg KB. Int J Fract 1968;4:11.
[36] Luna P, Bernal C, Cisilino A, Frontini P, Cotterell B, Mai Y-W. Polymer 2003;44:1145–50.
[37] Wu J, Mai Y-W, Cotterell B. J Mater Sci 1993;28:3373–84.
[38] Paton CA, Hashemi S. J Mater Sci 1992;27:2279–90.
[39] Marchal Y, Delannay F. Mater Sci Tech 1998;14:1163–8.
[40] Mai Y-W, Powell P. J Polym Sci, Part B: Polym Phys 1991;29:785–93.
[41] Bird RB, Armstrong RC, Hassager O. Dynamics of polymeric liquids. Fluid mechanics. vol. 1 1977.
[42] Rohlfing DC, Janzen J. Metallocene-based Polyolefins 2000;2:419–34.
[43] Hsieh ET, Tso CC, Byers JD, Johnson TW, Fu Q, Cheng SZD. J Macromol Sci Phys 1997;B36:615–28.
[44] DesLauriers PJ, Rohlfing DC, Hsieh ET. Polymer 2002;43:159–70.
[45] Sukhadia AM. J Plast Film Sheeting 1994;10:213.
[46] Failla M, Alamo RG, Mandelkern L. Polym Test 1992;11:151–9.
[47] Glotin M, Mandelkern L. Colloid Polym Sci 1982;260:182–92.
[48] Hansen EW, Kristiansen PE, Pedersen B. J Phys Chem B 1998;102:5444–50.
[49] Pake GE. J Chem Phys 1948;16:327–36.
[50] Look DC, Lowe IJ, Northby JA. J Chem Phys 1966;44:3441–52.

[51] Hsieh ET, Randall JC. Macromolecules 1982;15:1402–6.
[52] Hsieh ET, Randall JC. Macromolecules 1982;15:353–60.
[53] Fonseca CA, Harrison IR. Thermochim Acta 1998;313:37–41.
[54] Yau WW, Gillespie D. Polymer 2001;42:8947–58.
[55] Tso CC, DesLauriers PJ. Polymer 2004;45:2657–63.
[56] Pepper RE, Samuels RJ. In Encyclopedia of Polymer Science and Engineering, Wiley, NY, 1988;14:261–98.
[57] Hamada F, Wunderlich B, Sumida T, Hayashi S, Nakajima A. J Phys Chem 1968;72:178–85.
[58] Yoon DY, Cho TY, Shin EJ, Jeong W, Heck B, Strobl G, et al. Polym Mater Sci Eng 2004;91:242–3.
[59] Stein RS, Plaza A. J Polym Sci 1960;45:519–20.
[60] Clark RJ, Miller RL, Stein RS, Wilson PR. J Polym Sci 1960;42: 275–7.
[61] Wilkes GL, Stein RS. Structure and properties of oriented polymers. 2nd ed 1997.
[62] Chum PS, Kruper WJ, Guest MJ. J Adv Mater 2000;12:1759–67.
[63] Bubeck RA. Mater Sci Eng 2002;39:1–28.
[64] Herman JN, Biesenberger JA. Polym Eng Sci 1966;6:341–8.
[65] Clutton EQ, Rose LJ, Capaccio G. Plast Rubber Compos Process Appl 1998;27:478–82.
[66] Huang YL, Brown N. J Polym Sci, Part B: Polym Phys 1991;29: 129–37.